Supporting Information

Connecting the oxidative potential of fractionated particulate matter with chromophoric substances

Na Wu[1], Bingqing Lu[1], Qingcai Chen[2], Jianmin Chen[1], Xiang Li[*,1]

[1]*Department of Environmental Science & Engineering, Fudan University, Shanghai 200032, P.R. China*

[2]*School of Environmental Science and Engineering, Shaanxi University of Science and Technology, Xi'an 710021, P.R. China*

Correspondence to: Xiang Li (lixiang@fudan.edu.cn)

**Corresponding author.*

Number of Page	24
Number of Figures	9
Number of Tables	7

This document contains the following supporting information:

S1. Chemicals
S2. Chemical Analysis
S3. Potential source contribution function (PSCF)

Table S1. DTT_v activity normalized by volume (nmol/min/m^3)
Table S2. DTT_m activity normalized by PM mass (nmol/min/μg).
Table S3. Average DTT_v (nmol/min/m^3) and DTT_m (pmol/min/μg) of water-soluble extracts from ambient $PM_{2.5}$ at different locations all over the world.
Table S4. The seasonal variation of TFV (R.U.nm^2) of four chromophores.
Table S5. Regression equations of ·DTT loss rate from individual metals.
Table S6. Seasonal variation of chemical composition concentration of WSM (WSOC, OC, EC, and ions μg/m^3, elements, ng/m^3).
Table S7. Spearman correlation coefficient (r) of DTT activity with chemical composition of $PM_{2.5}$.

Figure S1. (A) Dithiothreitol (DTT) oxidation by redox active species in PM with subsequently ROS formation. (B) DTT reaction with 5,5'-dithio-bis (2-nitrobenzoic acid) (DTNB).
Figure S2. Seasonal variations of potential source regions for water-soluble DTT_v in Shanghai $PM_{2.5}$ (based on 48h backward trajectory).
Figure S3. Seasonal variations in the DTT consumption rate. DTT_v is the DTT consumption rate per cubic meter of atmospheric volume. DTT_m is the DTT consumption rate per microgram of $PM_{2.5}$.
Figure S4. Average DTT_v (nmol/min/m^3) a nd DTT_m (pmol/min/μg) of water-soluble extracts from ambient $PM_{2.5}$ at different locations in China (A) and (B) other countries all over the world.
Figure S5. The frequency distributions of the Pearson's correlation coefficients between different sample EEMs are calculated from the EEM pixel data points of the WSM and MSM.
Figure S6. Error comparison of C3 – C6 model results in PARAFAC analysis. The bold green dotted line indicates the number of factors selected in the study.
Figure S7. Split-half validation of the four-component model. Spectra were derived from two independent models of fluorescence EEM from two randomly split halves (with respect to samples) and matched to similar components in the model of the entire data set. The solid and dashed lines represent the spectra against excitation and emission wavelengths respectively.
Figure S8. (A) Relative contributions of four components to the total fluorescent volume. (B) Relative contributions of the fluorescent volumes of the WSM and MSM.
Figure S9. DTT loss rates as a function of concentration of individual metals. Lines represent regression fits to the experimental data; and the error bar represent the 95% confidence interval of DTT activity.

S1. Chemicals

The following chemicals were purchased from Sigma-Aldrich (Shanghai, China): sodium phosphate monobasic (NaH2PO4), sodium phosphate dibasic (Na2HPO4), DL-Dithiothreitol (DTT, 99.0%), 5,5'-dithiobis (2-nitrobenzoic acid) (DTNB, ReagentPlus, 99%), tris (hydroxymethyl) aminomethane (Tris, ACS reagent, 99.8%), ethylenediaminetetraacetic acid (EDTA, 99.995%), trischloroacetic acid (TCA, ACS reagent, 99.0%), methanol (MeOH). Nitric acid (HNO_3, 69%) and hydrofluoric acid (HF, 49%) were from Tansoole (Shanghai, China).

S2 UV-visible absorption spectra and EEM fluorescence spectra

The UV-visible absorption spectra of extracts were measured by Microplate Reader (BioTek Synergy™ HTX, Vermont, USA) between 200 and 800 nm with an interval of 5 nm in a 96-well quartz plate. The light absorption coefficient of the extracts at a given wavelength (Abs_λ, Mm^{-1}) can be calculated using eq1:

$$Abs_\lambda = (A_\lambda - A_{700}) \times \frac{V_{extraction}}{V_{air} \cdot l} \times \ln(10) \quad (1)$$

where $V_{extraction}$ (mL) is the volume of the extraction, V_{air} (m^3) related to the volume of air sampled through the filter during the sampling, l (cm) was the path length of light. A_λ at all wavelengths is referenced to A_{700} to account for systematic baseline drift.

The absorption Angstrom exponent (AAE) for each extract was an import parameter to describe the dependency of extracts' optical thickness on wavelength. It can be calculated using the Abs values between wavelength λ_1 and λ_2 (eq2):

$$AAE=\ln(\frac{Abs_{\lambda_1}}{Abs_{\lambda_2}})/\ln(\frac{\lambda_2}{\lambda_1}) \quad (2)$$

The excitation-emission matrix (EEM) spectra were measured using an Aqualog fluorimeter (Horiba-Jobin Yvon, Japan). The EEMs were measured in the range from 240 to 550 nm for excitation using 2 nm intervals and from 250 to 600 nm for emission at 3 nm intervals. The intensity of all EEM spectra was normalized by the area of the Raman water line obtained at 350 nm excitation and 397 nm emission wavelengths; the data were processed with inner-filter correction and Rayleigh scattering elimination. The EEM spectra were calibrated with Quinine sulfate standards, and the fluorescence intensities were expressed in units of quinine sulfate equivalents (QSE) (Coble, 1996). The fluorescence volume (FV, $R.U.nm^2$) of PM extracts was calculated using

florescence regional integration (FRI) (eq3) (Chen et al., 2003).

$$FV = \sum_{ex} \sum_{em} I(\lambda_{ex}\lambda_{em})\Delta\lambda_{ex}\Delta\lambda_{em} \quad (3)$$

S3. Chemical Analysis

Organic carbon (OC) and elemental carbon (EC) concentration of each sample were analysis by using a thermal/optical carbon analyzer (DRI Model 2001A, Atmoslytic Inc., Calabasas, CA, USA). A more detailed description of the analytical methods and calibration procedures are available in earlier paper(Feng et al., 2012). The water-soluble organic carbon (WSOC) was measured by total organic carbon analyzer (TOC-V CPH, Shimadzu, Japan). Water-soluble inorganic ions (Na^+, NH_4^+, K^+, Mg^{2+}, Ca^{2+}, Cl^-, NO_3^-, and SO_4^{2-}) were analyzed by ion chromatography (ICS-2000 and ICS-2500, DIONEX). Water-soluble metal (Pb, Mn, Zn, K, Cr, Fe, Ti, Sr, Al, Ca, Br, Ba, and Zr) in the particle samples were analyzed by using 7900 ICP-MS instrument (Agilent Technologies). Briefly, each samples were sonicated in 2mL of DI water for 1 h, after sonication, the extracts were filtered using PTFE 0.45 μm pore syringe filters, then HNO3 was added to produce a final concentration of 2% before ICP-MS (7900, Agilent Technologies) determination. In this study, we focus on Cu, Fe, and Mn as they are common redox active species linked to particle-generated ·OH. The signal response of a series of standard metal solutions (0.1-100 ppb) was recorded and the R^2 of the standard calibration curves ranged from 0.9991 to 0.9998 (N = 6) for the target metals.

S4. Potential source contribution function (PSCF)

PSCF modeling (Ashbaugh et al., 1985)was used to locate potential source areas contributing to the DTT activity. PSCF, defined as the conditional probability that the air mass reaching the receptor site after transport has a pollutant concentration above the given criterion, is given by

$$PSCF_{ij} = \frac{m_{ij}}{n_{ij}} \quad (1)$$

where n_{ij} is the total number of trajectory endpoints that fall in the ij_{th} grid cell during transportation to the receptor site, and m_{ij} is a subclass of n_{ij} whose trajectory endpoints are associated with the pollutant concentrations higher than the given criterion. The grid cells with high $PSCF_{ij}$ indicate regions of 'high potential'

contribution for the pollutant. Generally, $PSCF_{ij}$ values < 0.5 are considered to be low, whereas values of 0.5–1.0 are considered high.

To minimize high uncertainties caused by small n_{ij} values, a weighting function W_{ij} was applied to constrain the contribution from grids with a low number of trajectories. Based on the mean number of trajectory endpoints in each grid ($n_{av.}$), the weighting function W_{ij} (Polissar et al., 2001)is defined as

$$W_{ij} = \begin{cases} 1.00 & 3n_{ave} < n_{ij} \\ 0.70 & 1.5n_{ave} < n_{ij} < 3n_{ave} \\ 0.42 & 0.75n_{ave} < n_{ij} < 1.5n_{ave} \\ 0.17 & n_{ij} < 0.75n_{ave} \end{cases} \quad (4)$$

In PSCF analysis, a 48-h backward trajectory was calculated every 4 h to identify potential regional contributions of DTT_V. The analysis was initiated at an altitude of 500 m. The geophysical regions covered by the trajectories were split into 0.5° × 0.5° grid cells.

Table S1. DTT_v activity normalized by volume (nmol/min/m^3).

DTT_v (nmol/min/m^3)	Sampling date	WSM	MSM	WISM	Hydrophilic	Hydrophobic
Spring	Apr.12	4.62	4.47	2.20	3.11	3.31
	Apr.14	4.24	3.76	2.81	3.08	2.52
	Apr.15	3.29	2.34	3.08	2.53	2.64
	Apr.19	4.14	3.62	3.38	2.77	2.33
	Apr.25	4.32	3.42	2.30	3.16	2.96
	Apr.26	3.39	2.94	1.91	2.35	2.77
	Average	4.00±0.5	3.42±0.73	2.61±0.57	2.83±0.34	2.76±0.34
Summer	Jul.29	2.91	4.24	2.84	3.02	2.36
	Jul.30	3.32	3.56	3.13	3.02	2.87
	Jul.31	3.41	3.32	2.70	3.26	1.92
	Aug.01	3.18	3.93	2.54	2.63	2.08
	Aug.02	2.99	3.88	3.86	2.31	3.99
	Aug.06	4.01	4.17	3.04	2.41	3.53
	Average	3.30±0.39	3.85±0.36	3.02±0.46	2.77±0.38	2.79±0.83
Fall	Nov.10	3.89	2.66	1.96	2.50	3.01
	Nov.11	3.63	3.10	2.03	2.47	2.78
	Nov.13	4.06	2.73	2.21	2.86	2.65
	Nov.16	3.29	2.62	2.34	2.49	3.23
	Nov.18	3.47	2.59	1.76	2.97	3.07
	Nov.20	3.61	2.81	1.62	2.34	3.33
	Average	3.66±0.28	2.75±0.19	1.98±0.27	2.60±0.25	3.01±0.26
Winter	Dec.01	5.41	4.37	2.34	5.19	5.43
	Dec.02	7.25	5.88	3.23	6.96	4.18
	Dec.03	6.34	4.57	3.41	5.20	3.59
	Dec.07	5.17	3.51	3.28	4.74	3.50
	Dec.08	6.77	4.92	3.07	5.60	
	Dec.09	5.68	4.45	2.88	5.24	3.38
	Average	6.11±0.82	4.62±0.77	3.03±0.39	5.49±0.77	4.02±0.85

Table S2. DTT_m activity normalized by PM mass (nmol/min/μg).

DTT_m (nmol/min/μg)						
	Sampling date	**WSM**	**MSM**	**WISM**	**Hydrophilic**	**Hydrophobic**
Spring	Apr.12	0.11	0.11	0.05	0.07	0.08
	Apr.14	0.08	0.07	0.05	0.06	0.05
	Apr.15	0.12	0.08	0.11	0.09	0.10
	Apr.19	0.11	0.10	0.09	0.07	0.06
	Apr.25	0.10	0.00	0.05	0.07	0.07
	Apr.26	0.13	0.12	0.08	0.09	0.11
	Average	0.11±0.02	0.08±0.04	0.07±0.02	0.08±0.01	0.08±0.02
Summer	Jul.29	0.06	0.08	0.05	0.06	0.05
	Jul.30	0.06	0.07	0.06	0.06	0.05
	Jul.31	0.07	0.07	0.06	0.07	0.04
	Aug.01	0.07	0.09	0.06	0.06	0.05
	Aug.02	0.06	0.08	0.08	0.05	0.08
	Aug.06	0.06	0.07	0.05	0.04	0.06
	Average	0.06±0.01	0.08±0.01	0.06±0.01	0.05±0.02	0.05±0.01
Fall	Nov.10	0.06	0.04	0.03	0.04	0.04
	Nov.11	0.06	0.05	0.04	0.04	0.04
	Nov.13	0.07	0.05	0.04	0.05	0.05
	Nov.16	0.06	0.05	0.04	0.05	0.05
	Nov.18	0.06	0.05	0.03	0.04	0.05
	Nov.20	0.06	0.05	0.03	0.05	0.04
	Average	0.06±0.01	0.05±0.01	0.03±0.01	0.04±0.003	0.04±0.01
Winter	Dec.01	0.05	0.04	0.02	0.03	0.03
	Dec.02	0.05	0.04	0.02	0.03	0.02
	Dec.03	0.06	0.04	0.03	0.04	0.04
	Dec.07	0.05	0.04	0.03	0.04	0.04
	Dec.08	0.07	0.05	0.03	0.05	0.05
	Dec.09	0.06	0.05	0.03	0.06	0.05
	Average	0.06±0.01	0.04±0.01	0.03±0.01	0.04±0.01	0.04±0.01

Table S3. Average DTT_v (nmol/min/m^3) and DTT_m (nmol/min/μg) of water-soluble extracts from ambient $PM_{2.5}$ at different locations all over the world.

Area	Country	Site type	Sampling time	Category	Solvents	Filter	DTT_v (nmol/min/m^3)	DTT_m (nmol/min/μg)	Reference
Shanghai	China	Urban	April and December, 2019	$PM_{2.5}$	Water	Quartz	4.27±1.26 (average)	0.07±0.02	This study
					MeOH	Quartz	3.66±0.51	0.06±0.02	
Beijing	China	Urban	May 2015 to April 2016	$PM_{2.5}$	Water	Quartz	12.26±6.82 (mean)	0.13±0.10	(Yu et al., 2019)
Hangzhou	China	Urban	2017	$PM_{2.5}$	Water	Quartz	0.62±0.24 (median)	5.63 pmol/min/μg	(Wang et al., 2019)
Coastal cities of the Bohai Sea	China	coastal city	May 2015 to April 2016	$PM_{2.5}$	Water	Quartz	4.4±2.6 (Jizhou)	0.035 ± 0.018	(Liu et al., 2018)
							6.8±3.4 (Tianjin)	0.049 ± 0.016	
							4.2±2.7 (Yantai)	0.030 ± 0.016	
Hong Kong	China	Urban	September 6, 2011, to August 16, 2012	$PM_{2.5}$	Water	Teflon	0.52±0.08	38.5 pmol	(Cheng et al., 2020)
Wuhan	China	Urban	Oct. 2011 to July 2012	$PM_{2.5}$	Water	Quartz	1.8±0.2	41.65 pmol	(Liu et al., 2020)
Sichuan	China	Urban	September and December of 2012	$PM_{2.5}$	Water	Quartz	2.71 (1.95–3.28)	/	(Secrest et al., 2016)
Chifeng	China	Urban					5.32 (0.725–12.5)		
Guangzhou		Urban	Dec. 2017 to May 2018	$PM_{2.5}$	Water	Quartz	4.46	14.07 pmol/min/μg	(Man-Man et al., 2019)
Rotterdam	Netherlands	Urban	Aug. to Nov. 2011		Water	Quartz	2.3±1.3	/	(Yang et al., 2014)
					Water	Teflon	2.2±1.3		
					MeOH	Teflon	2.9±1.7		
Xi'an	China	Urban	2017	$PM_{2.5}$	Water	Quartz	0.53 (spring)	11.7 pmol/min/μg	(Chen et al., 2019; Wang et al., 2020)
							0.50(summer)	15.67	
							0.40(fall)	6.94	
							0.64 (winter)	6.89	
Tehran	Iran	Urban	February 2014 to January 2015	$PM_{2.5}$	Water	Teflon	2.1−9.3	/	(Al Hanai et al., 2019)
Bologna	Italy	Urban	Autumn, 2011; summer to winter, 2012; winter to autumn, 2013; winter to spring, 2014	$PM_{2.5}$	Water	Quartz	≈0.3 to 1.7	0.03 (mean)	(Visentin et al., 2016)
Toronto	Canada		summer 2016 and winter 2017	$PM_{2.5}$	Water	Teflon	0.31	/	(Weichenthal et al., 2019)

Rotterdam	Netherlands	Urban	March to October 2009	$PM_{2.5}$	MeOH	Teflon	1.4	0.03-0.18	(Janssen et al., 2014)
Lecce	Italy	Urban	Autumn and winter, 2013 and 2016	$PM_{2.5}$	Water	Quartz	0.40 ±0.26	14.5 ±7.6 pmol/min/μg	(Chirizzi et al., 2017)
Bangalore	India	Remote	October 2013	$PM_{2.5}$	Water	Quartz	0.79 ±0.13	107 ± 25 pmol/min/μgOC	(Vreeland et al., 2016)
Punjab	India	Urban	January 10th to February 3rd, 2014	$PM_{2.5}$	Water	Quartz	3.8 ±1.4	26.6 ±8.4 pmol	(Patel et al., 2018)
Delhi	India	Urban	Real-time	$PM_{2.5}$	Water	Quartz	1.57 ±0.7	/	(Puthussery et al., 2020)
Guanggju	Korea	Urban	2016 10-2017 1	$PM_{2.5}$	Water	Zefluor	~1	31.6 pmol/min/μg	(Borlaza et al., 2018)
		Rural					~0.5		
Manila Metropolitan	Philippines	Urban	2016 1-2016 10				2	/	
Atlanta	USA	Urban/Rural	June 2012 to September 20132	$PM_{2.5}$	Water	Quartz	0.1–1.5	0.005–0.1	(Verma et al., 2014)
Oslo	Norway	Urban/Rural	05.02.2009-29.01.2010	$PM_{2.5}$	Water	Quartz	0.06-0.25	/	(Jedynska et al., 2017)
Helsinki/Turku	Finland		27.01.2010-26.01.2011				0.09-0.43		
London/Oxford	United Kingdom		26.01.2010-18.01.2011				0.08-0.19		
Copenhagen	Denmark		19.11.2009-17.11.2010				0.08-0.31		
Rotterdam	Netherlands		17.02.2009-19.02.2010				0.13-0.29		
Munich/Augsburg	Germany		17.02.2009-19.02.2010				0.20 (mean)		
Catalonia	Spain		14.01.2009-14.01.2010				0.23 (mean)		
Paris	France		04.01.2010-04.01.2011				0.1-0.36		
Roma	Italy		27.01.2010-26.01.2011				0.11-0.34		
Athens	Greece		21.04.2010-27.04.2011				0.1-1.5		
Los Angeles	USA	Urban	October 24, October 25, October 27, November 1, November 14, 2007	$PM_{2.5}$	Water	Teflon	0.62±0.21	0.024±0.005	(Verma et al., 2009)

Table S4. The seasonal variation of TFV (R.U.nm^2) of four chromophores.

	WSM					MSM			
TFV (R.U.nm^2)	**C1**	**C2**	**C3**	**C4**	**TFV (R.U.nm^2)**	**C1**	**C2**	**C3**	**C4**
	32.60	102.97	242.29	1.06		31.54	983.78	629.45	748.48
	29.92	731.72	601.62	486.84		26.53	798.59	677.56	554.93
Spring	23.22	89.05	223.98	24.31	Spring	16.51	810.21	363.27	659.01
	29.21	117.70	246.91	4.57		25.54	945.42	520.64	687.69
	30.48	100.79	228.46	10.64		24.13	907.13	662.98	621.15
	23.92	101.53	243.45	22.22		20.75	981.23	495.54	772.58
Average	28.23	207.29	297.78	91.61	Average	24.17	904.40	558.24	673.97
SD	3.79	257.08	149.12	193.85	SD	5.14	82.42	121.36	80.81
	20.53	68.41	95.81	0.00		23.43	27.59	68.46	16.77
	24.06	47.13	69.80	1.80	Summer	27.73	37.55	76.60	4.92
Summer	22.44	37.57	48.18	0.00	Average	25.58	32.57	72.53	10.84
	21.10	40.57	43.93	0.00	SD	3.04	7.04	5.76	8.38
	28.30	47.70	68.23	0.00		18.77	167.99	387.78	129.16
Average	20.04	83.08	79.18	32.61		21.87	77.05	192.45	55.43
SD	8.43	85.92	38.94	78.99	Fall	19.26	190.00	380.49	86.51
	28.65	146.45	291.34	32.42		18.49	154.73	311.85	73.55
Fall	23.22	137.26	260.23	34.69		18.28	199.26	434.07	110.38
	24.49	184.54	364.81	58.71		19.83	249.95	508.42	143.51
	25.47	183.18	358.98	52.08	Average	19.42	173.16	369.18	99.76
Average	21.72	136.74	232.24	48.25	SD	1.33	57.38	108.25	33.82
SD	7.09	44.72	140.50	18.70		30.84	976.33	1035.55	700.22
	38.17	335.51	721.90	135.03		41.49	1456.12	1950.00	964.19
	51.16	510.64	1145.77	255.39	Winter	32.25	1477.16	2183.10	1013.87
Winter	44.74	469.96	1075.02	248.94		24.77	779.55	832.86	552.99
	36.48	394.84	828.16	158.75		34.72	392.97	375.75	288.57
	47.77	393.43	854.27	160.15		31.40	1071.27	1356.19	693.10
	40.08	339.97	721.22	138.38	Average	32.58	1025.57	1288.91	702.16
Average	43.07	407.39	891.06	182.78	SD	5.47	413.41	685.15	268.03
SD	5.77	70.20	179.72	54.75					

Table S5. Regression equations of ·DTT loss rate from individual metals.

Compounds	Range of tested concentration (μM)	Regression equations	R^2	N[a]
Fe	0.5, 1, 2.5, 4, 8, 10	$y=0.08x+0.47$	0.94	6
Mn	0.1, 0.5, 1, 2.5, 4, 5	$y=1.78x^{0.09}$	0.95	6
Cu	0.1, 0.5, 1, 2.5, 4, 5, 10	$y=1.94x^{0.07}$	0.97	7

[a] Number of different concentrations used in used in the regression equations.

Table S6. Seasonal variation of chemical composition concentration of WSM (WSOC, OC, EC, and ions μg/m^3, elements, ng/m^3).

	Spring		Summer		Fall		Winter	
	Mean	**SD**	**Mean**	**SD**	**Mean**	**SD**	**Mean**	**SD**
WSOC	3.44	0.57	3.35	0.75	3.45	0.76	6.40	1.61
OC	5.48	1.48	2.90	1.18	3.65	1.07	13.32	4.12
EC	3.44	0.97	1.23	1.51	2.88	0.88	6.46	1.01
Cl^-	0.32	0.22	0.16	0.04	0.77	0.23	1.26	0.47
Br^-	0.31	0.05	0.25	0.11	0.21	0.01	0.38	0.08
NO_3^-	8.91	5.62	0.62	0.08	2.47	0.67	35.43	13.18
SO_4^{2-}	5.54	1.92	2.30	1.70	3.13	0.33	8.85	2.66
PO_4^{2-}	0.87	0.15	1.01	0.07	1.88	0.09	1.55	0.09
Na^+	0.58	0.08	0.65	0.07	2.25	0.20	2.22	0.15
NH_4^+	3.91	2.20	0.48	0.63	0.96	0.20	11.39	3.73
K^+	0.13	0.07	0.02	0.03	0.13	0.05	0.59	0.18
Ca^{2+}	1.47	0.34	2.11	0.33	2.62	0.71	1.92	0.28
Mg^{2+}	0.27	0.04	0.41	0.06	0.50	0.07	0.29	0.03
V	0.04	0.02	0.04	0.01	0.04	0.02	0.05	0.01
Mn	0.12	0.01	0.08	0.07	0.14	0.10	0.37	0.10
Cu	0.85	0.99	0.39	0.24	0.29	0.15	0.93	0.57
Fe	2.93	2.70	3.15	2.52	5.57	3.15	12.69	6.17
Co	0.24	0.24	0.19	0.08	0.09	0.04	0.25	0.15
Mg	30.03	9.39	59.67	25.01	86.91	100.04	48.27	26.10
Al	7.31	7.17	17.88	3.86	18.19	9.37	19.98	8.82
Ca	31.99	7.97	73.45	33.26	95.53	113.06	56.96	27.30

Table S7. Spearman's correlation coefficient (r) between DTT_v and $PM_{2.5}$ components.

	DTT_v (WSM)	**DTT_v (MSM)**
WSOC	0.80**	0.61**
OC	0.85**	0.47*
EC	0.87**	0.43*
Cl^-	0.59**	0.02
Br^-	0.63**	0.62**
NO_3^-	0.84**	0.41*
SO_4^{2-}	0.87**	0.48*
PO_4^{2-}	0.10	-0.33
Na^+	0.27	-0.12
NH_4^+	0.86**	0.50*
K^+	0.81**	0.30
Ca^{2+}	-0.26	-0.25
Mg^{2+}	-0.55	-0.46*
V	0.33	0.40
Mn	0.92**	0.49*
Cu	0.61**	0.40
Fe	0.53**	0.33
Co	0.25	0.35
Mg	-0.29	-0.07
Al	0.16	0.18
Ca	-0.29	-0.03

** Correlation is significant at 0.01 level (2-tailed).
* Correlation is significant at 0.05 level (2-tailed).

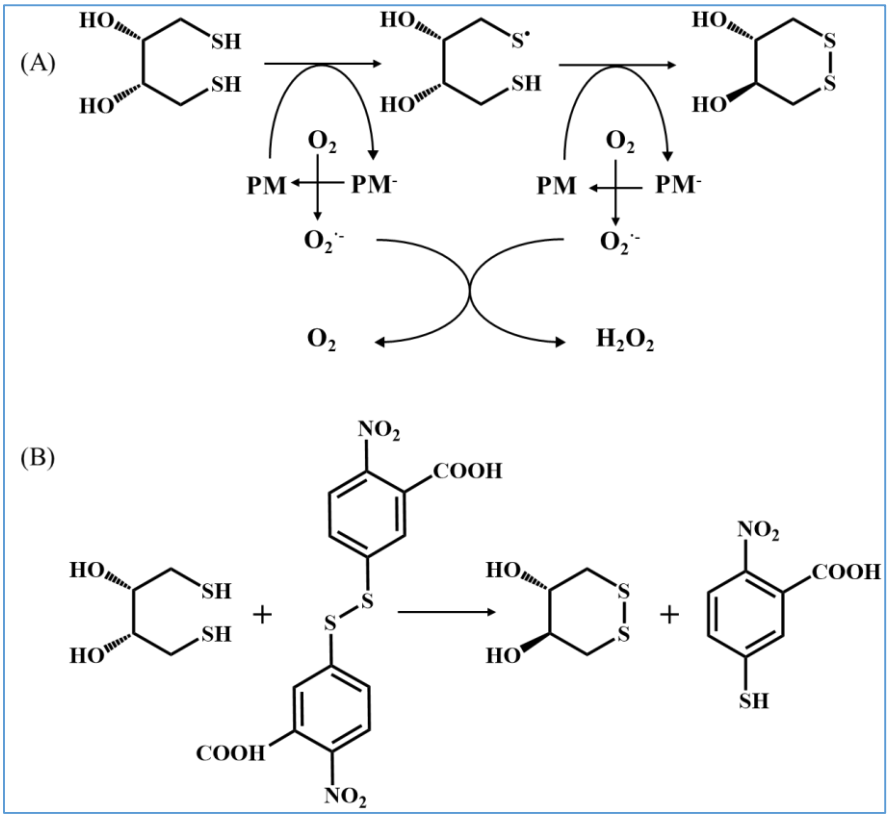

Figure S1. (A) Dithiothreitol (DTT) oxidation by redox active species in PM with subsequently ROS formation. (B) DTT reaction with 5,5'-dithio-bis (2-nitrobenzoic acid) (DTNB).

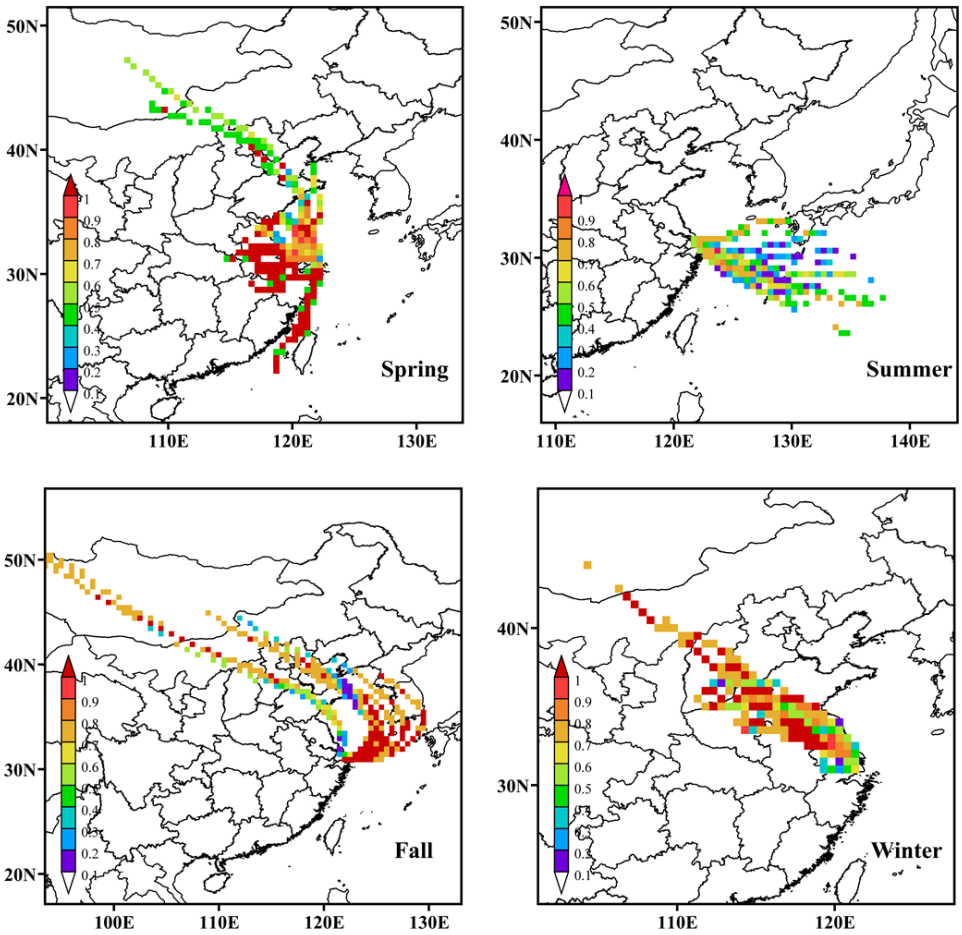

Figure S2. Seasonal variations of potential source regions for water-soluble DTT_v in Shanghai $PM_{2.5}$ (based on 48h backward trajectory).

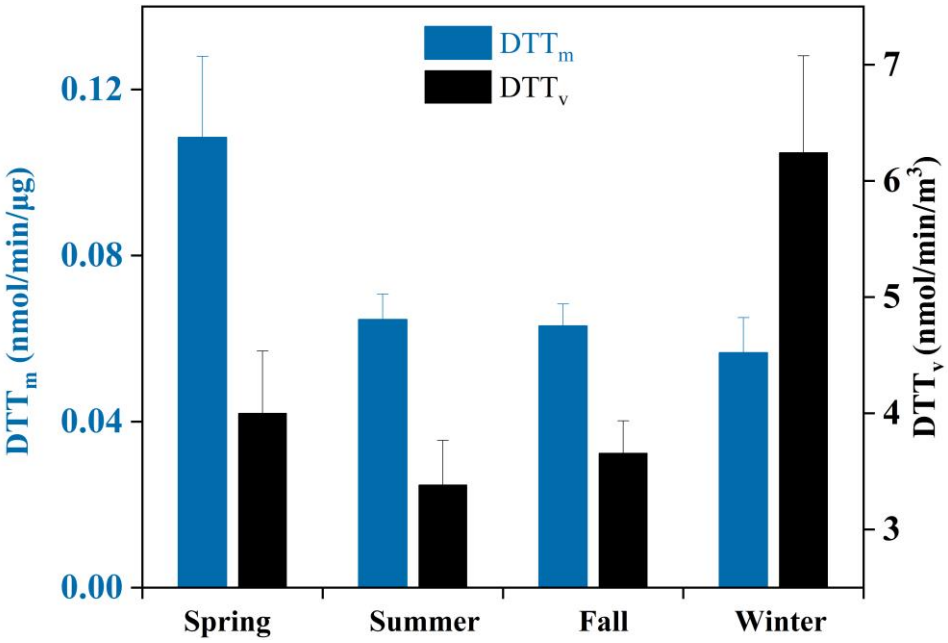

Figure S3. Seasonal variations in the DTT consumption rate. DTT_v is the DTT consumption rate per cubic meter of atmospheric volume. DTT_m is the DTT consumption rate per microgram of $PM_{2.5}$.

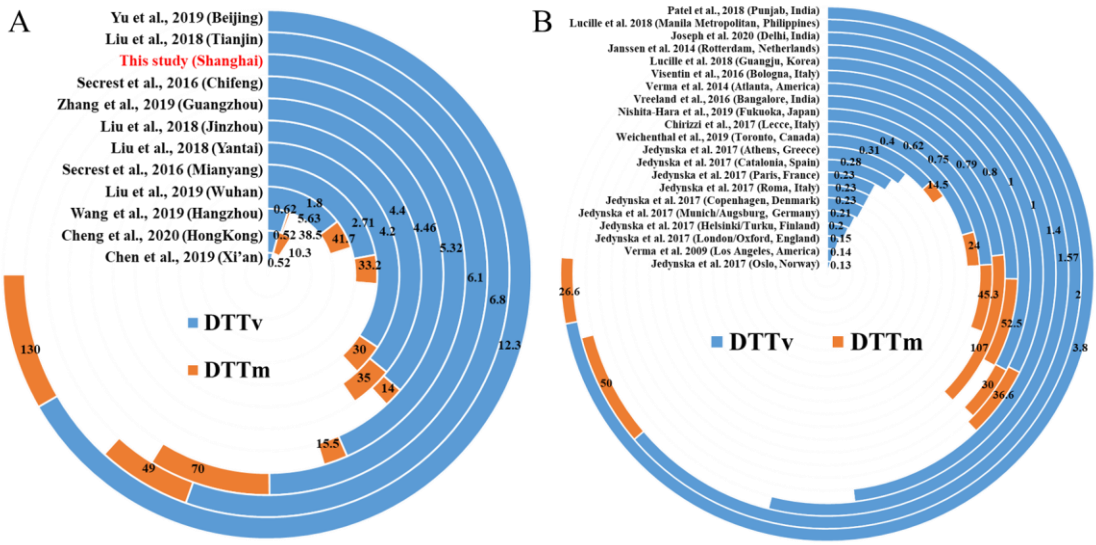

Figure S4. Average DTT_v (nmol/min/m3) and DTT_m (pmol/min/μg) of water-soluble extracts from ambient $PM_{2.5}$ at different locations in China (A) and (B) other countries all over the world.

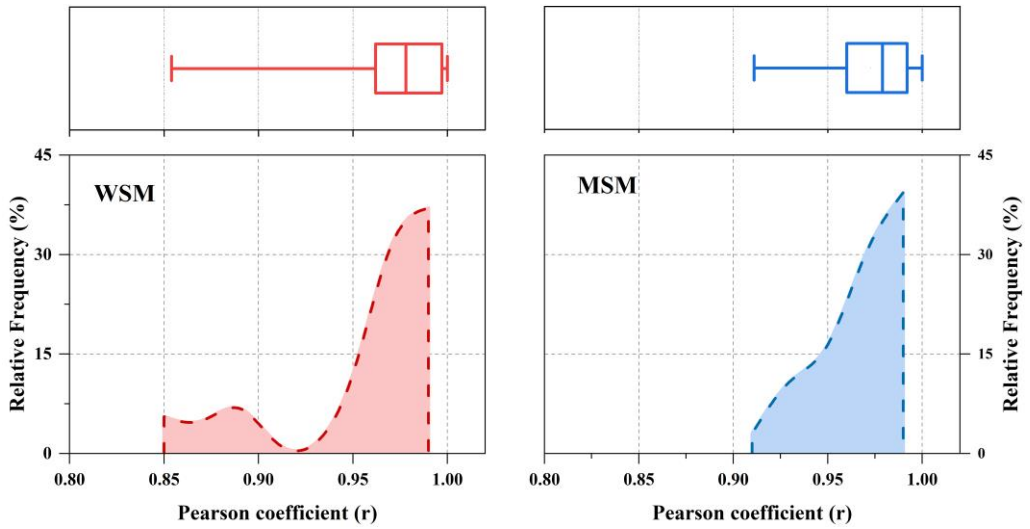

Figure S5. The frequency distributions of the Pearson's correlation coefficients between different sample EEMs are calculated from the EEM pixel data points of the WSM and MSM.

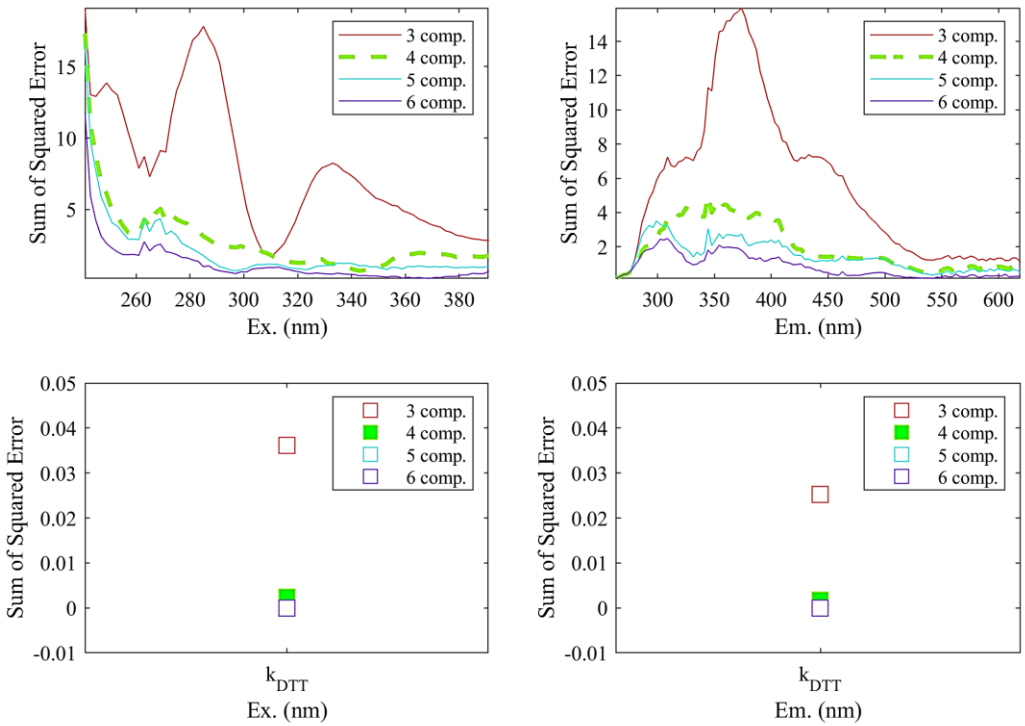

Figure S6. Error comparison of C3 – C6 model results in PARAFAC analysis. The bold green dotted line indicates the number of factors selected in the study.

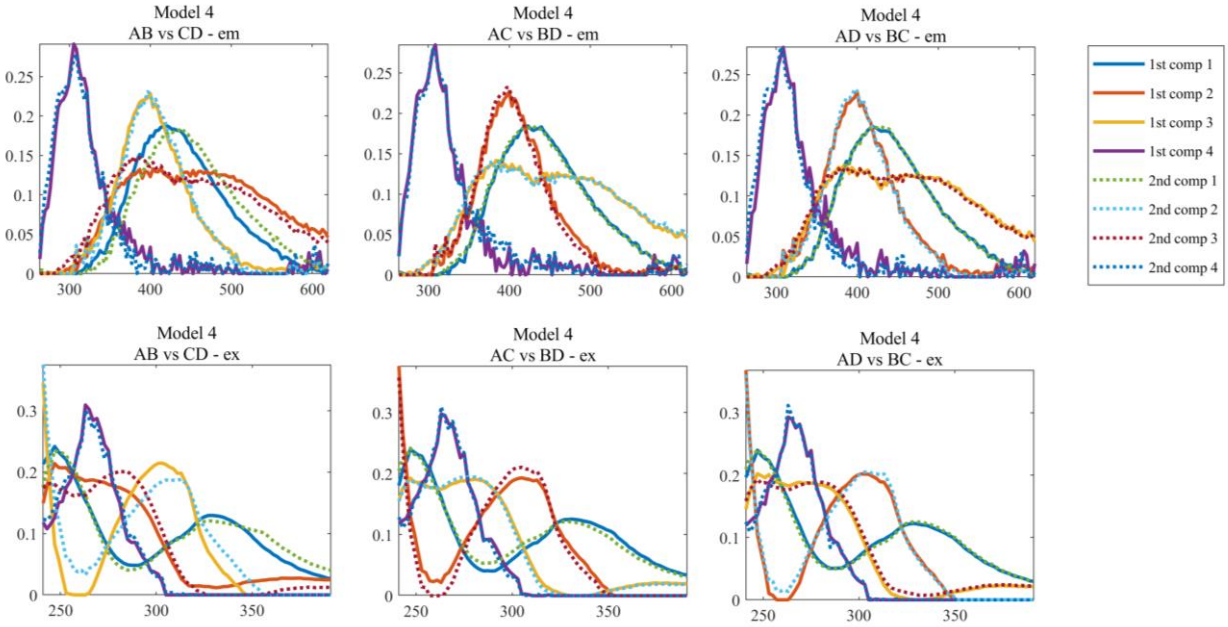

Figure S7. Split-half validation of the four-component model. Spectra were derived from two independent models of fluorescence EEM from two randomly split halves (with respect to samples) and matched to similar components in the model of the entire data set. The solid and dashed lines represent the spectra against excitation and emission wavelengths respectively.

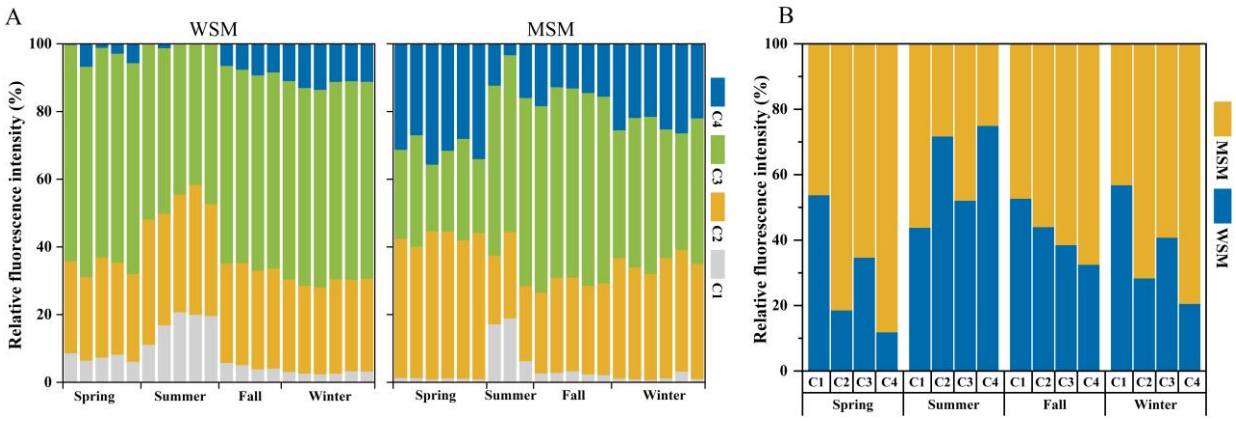

Figure S8. (A) Relative contributions of four components to the total fluorescent volume. (B) Relative contributions of the fluorescent volumes of the WSM and MSM.

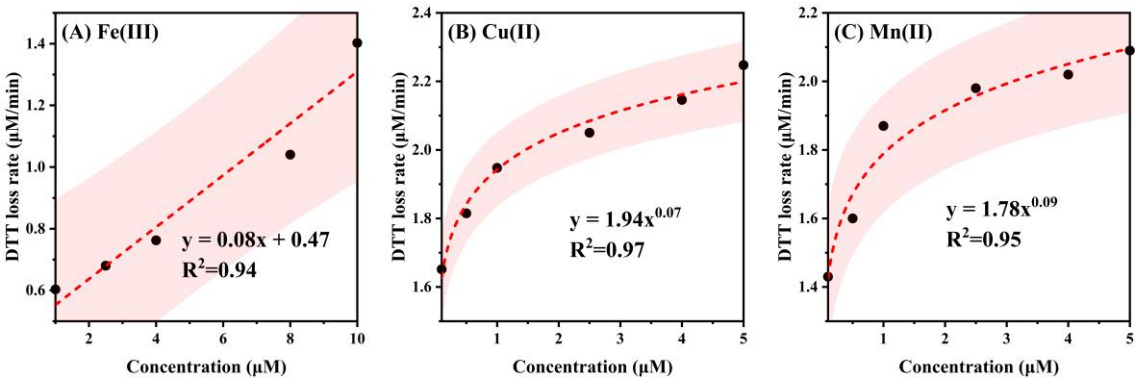

Figure S9. DTT loss rates as a function of concentration of individual metals. Lines represent regression fits to the experimental data; and the error bar represent the 95% confidence interval of DTT activity.

References

Al Hanai, A. H., D. S. Antkiewicz, J. D. C. Hemming, M. M. Shafer, A. M. Lai, M. Arhami, V. Hosseini, and J. J. Schauer (2019), Seasonal variations in the oxidative stress and inflammatory potential of PM2.5 in Tehran using an alveolar macrophage model; The role of chemical composition and sources, *Environment International*, *123*, 417-427, doi:https://doi.org/10.1016/j.envint.2018.12.023.

Ashbaugh, L. L., W. C. Malm, and W. Z. Sadeh (1985), A residence time probability analysis of sulfur concentrations at grand Canyon National Park, *Atmospheric Environment (1967)*, *19*(8), 1263-1270, doi:https://doi.org/10.1016/0004-6981(85)90256-2.

Borlaza, L. J. S., E. M. R. Cosep, S. Kim, K. Lee, H. Joo, M. Park, D. Bate, M. G. Cayetano, and K. Park (2018), Oxidative potential of fine ambient particles in various environments, *Environmental Pollution*, *243*, 1679-1688, doi:https://doi.org/10.1016/j.envpol.2018.09.074.

Chen, Q., M. Wang, Y. Wang, L. Zhang, Y. Li, and Y. Han (2019), Oxidative Potential of Water-Soluble Matter Associated with Chromophoric Substances in PM2.5 over Xi'an, China, *Environmental Science and Technology*, doi:10.1021/acs.est.9b01976.

Chen, W., P. Westerhoff, J. A. Leenheer, and K. Booksh (2003), Fluorescence Excitation−Emission Matrix Regional Integration to Quantify Spectra for Dissolved Organic Matter, *Environmental Science and Technology*, *37*(24), 5701-5710, doi:10.1021/es034354c.

Cheng, Y., Y. Ma, B. Dong, X. Qiu, and D. Hu (2020), Pollutants from primary sources dominate the oxidative potential of water-soluble PM2.5 in Hong Kong in terms of dithiothreitol (DTT) consumption and hydroxyl radical production, *Journal of Hazardous Materials*, 124218, doi:https://doi.org/10.1016/j.jhazmat.2020.124218.

Chirizzi, D., D. Cesari, M. R. Guascito, A. Dinoi, L. Giotta, A. Donateo, and D. Contini (2017), Influence of Saharan dust outbreaks and carbon content on oxidative potential of water-soluble fractions of PM2.5 and PM10, *Atmospheric Environment*, *163*, 1-8, doi:https://doi.org/10.1016/j.atmosenv.2017.05.021.

Coble, P. G. (1996), Characterization of marine and terrestrial DOM in seawater using excitation-emission matrix spectroscopy, *Marine Chemistry*, *51*(4), 325-346.

Feng, J., P. Sun, X. Hu, W. Zhao, M. Wu, and J. Fu (2012), The chemical composition and sources of PM2.5 during the 2009 Chinese New Year's holiday in Shanghai, *Atmospheric Research*, *118*, 435-444, doi:https://doi.org/10.1016/j.atmosres.2012.08.012.

Janssen, N. A., A. Yang, M. Strak, M. Steenhof, B. Hellack, M. E. Gerlofs-Nijland, et al. (2014), Oxidative potential of particulate matter collected at sites with different source characteristics, *Science of the Total Environment*, *472*, 572-581, doi:10.1016/j.scitotenv.2013.11.099.

Jedynska, A., G. Hoek, M. Wang, A. Yang, M. Eeftens, J. Cyrys, et al. (2017), Spatial variations and development of land use regression models of oxidative potential in ten European study areas, *Atmos. Environ.*, *150*, 24.

Liu, Q., Z. Lu, Y. Xiong, F. Huang, J. Zhou, and J. J. Schauer (2020), Oxidative potential of ambient PM2.5 in Wuhan and its comparisons with eight areas of China, *Science of the Total Environment*, *701*, 134844, doi:https://doi.org/10.1016/j.scitotenv.2019.134844.

Liu, W. J., Y. Xu, W. Liu, Q. Liu, S. Yu, Y. Liu, X. Wang, and S. Tao (2018), Oxidative potential of ambient PM 2.5 in the coastal cities of the Bohai Sea, northern China: Seasonal variation and source apportionment, *Environmental Pollution*, *236*, 514-528.

Man-Man, Z., L. I. Hui-Rong, Y. Wen-Da, S. Jia-Yin, W. U. Cheng, C. Peng, and T. Ming-Jin (2019), Measurement based on DTT method of the PM_(2.5) oxidative potential in Guangzhou urban area, *China Environmental Science*.

Patel, A., and N. Rastogi (2018), Oxidative potential of ambient fine aerosol over a semi-urban site in the Indo-Gangetic Plain, *Atmospheric Environment*, *175*, 127-134, doi:https://doi.org/10.1016/j.atmosenv.2017.12.004.

Polissar, A. V., P. K. Hopke, and J. M. Harris (2001), Source Regions for Atmospheric Aerosol Measured at Barrow, Alaska, *Environmental Science and Technology*, *35*(21), 4214-4226, doi:10.1021/es0107529.

Puthussery, J. V., A. Singh, P. Rai, D. Bhattu, V. Kumar, P. Vats, et al. (2020), Real-Time Measurements of PM2.5 Oxidative Potential Using a Dithiothreitol Assay in Delhi, India, *Environmental Science & Technology Letters*, *7*(7), 504-510, doi:10.1021/acs.estlett.0c00342.

Secrest, M. H., J. J. Schauer, E. M. Carter, A. M. Lai, Y. Wang, M. Shan, X. Yang, Y. Zhang, and J. Baumgartner (2016), The oxidative potential of PM2.5 exposures from indoor and outdoor sources in rural China, *Science of the Total Environment*, *571*, 1477-1489, doi:https://doi.org/10.1016/j.scitotenv.2016.06.231.

Verma, V., T. Fang, H. Guo, L. King, J. T. Bates, R. E. Peltier, E. Edgerton, A. G. Russell, and R. J. Weber (2014), Reactive oxygen species associated with water-soluble PM2.5 in the southeastern United States:

spatiotemporal trends and source apportionment, *Atmospheric Chemistry and Physics,14,23(2014-12-08)*, *14*(13), 19625-19672.
Verma, V., A. Polidori, J. J. Schauer, M. M. Shafer, F. R. Cassee, and C. Sioutas (2009), Physicochemical and Toxicological Profiles of Particulate Matter in Los Angeles during the October 2007 Southern California Wildfires, *Environmental Science and Technology*, *43*(3), 954-960, doi:10.1021/es8021667.
Visentin, M., A. Pagnoni, E. Sarti, and M. C. Pietrogrande (2016), Urban PM2.5 oxidative potential: Importance of chemical species and comparison of two spectrophotometric cell-free assays, *Environmental Pollution*, *219*, 72-79, doi:10.1016/j.envpol.2016.09.047.
Vreeland, H., J. J. Schauer, A. G. Russell, J. D. Marshall, A. Fushimi, G. Jain, K. Sethuraman, V. Verma, S. N. Tripathi, and M. H. Bergin (2016), Chemical characterization and toxicity of particulate matter emissions from roadside trash combustion in urban India, *Atmospheric Environment*, *147*, 22-30, doi:https://doi.org/10.1016/j.atmosenv.2016.09.041.
Wang, J., X. Lin, L. Lu, Y. Wu, H. Zhang, Q. Lv, W. Liu, Y. Zhang, and S. Zhuang (2019), Temporal variation of oxidative potential of water soluble components of ambient PM2.5 measured by dithiothreitol (DTT) assay, *Science of the Total Environment*, *649*, 969-978, doi:https://doi.org/10.1016/j.scitotenv.2018.08.375.
Wang, Y., M. Wang, S. Li, H. Sun, Z. Mu, L. Zhang, Y. Li, and Q. Chen (2020), Study on the oxidation potential of the water-soluble components of ambient PM2.5 over Xi'an, China: Pollution levels, source apportionment and transport pathways, *Environment International*, *136*, 105515, doi:https://doi.org/10.1016/j.envint.2020.105515.
Weichenthal, S., M. Shekarrizfard, A. Traub, R. Kulka, K. Al-Rijleh, S. Anowar, G. J. Evans, and M. Hatzopoulou (2019), Within-City Spatial Variations in Multiple Measures of PM2.5 Oxidative Potential in Toronto, Canada, *Environmental Science and Technology*, doi:10.1021/acs.est.8b05543.
Yang, A., A. Jedynska, B. Hellack, I. Kooter, G. Hoek, B. Brunekreef, T. A. J. Kuhlbusch, F. R. Cassee, and N. A. H. Janssen (2014), Measurement of the oxidative potential of PM2.5 and its constituents: The effect of extraction solvent and filter type, *Atmospheric Environment*, *83*, 35-42, doi:https://doi.org/10.1016/j.atmosenv.2013.10.049.
Yu, S., W. Liu, Y. Xu, K. Yi, M. Zhou, S. Tao, and W. Liu (2019), Characteristics and oxidative potential of atmospheric PM2.5 in Beijing: Source apportionment and seasonal variation, *Science of the Total Environment*, *650*, 277-287, doi:https://doi.org/10.1016/j.scitotenv.2018.09.021.